Methods for Electromagnetic Scattering by Large Axisymmetric Particles with Extreme Geometries

Adrian Doicu, Yuri Eremin, Dmitry S. Efremenko and Thomas Trautmann

Abstract Several methods for electromagnetic scattering by large axisymmetric particles with extreme geometries are analyzed. These include the discrete sources method and the null-field method with distributed and multiple spherical vector wave functions, as well as, a single spherical coordinate-based null-field method equipped with an analytical approach for computing the elements of the transition matrix. The numerical performances of the methods with distributed and multiple spherical vector wave functions are illustrated through simulations for spheroids and cylinders.

3.1 Introduction

Accurate computation of electromagnetic scattering by large axisymmetric particles with extreme geometries is needed in atmospheric radiative transfer and remote sensing to analyze the parameters of radiation scattered by aerosols, clouds, and precipitations. In the last years, the discrete sources method and the null-field method have become efficient and powerful tools for rigorously computing the electromagnetic scattering by such kind of scatterers.

1. In the discrete sources method, the approximate solution to the scattering problem is written as a superposition of fields of elementary (discrete) sources. The discrete sources, consisting of localized, distributed and multiple spherical vector wave functions, magnetic and electric dipoles, and systems of vector Mie potentials, are placed on a certain support, while the unknown amplitudes of the discrete sources are determined from the boundary conditions [1–4].

A. Doicu (✉) · D. S. Efremenko · T. Trautmann
Remote Sensing Technology Institute, German Aerospace Centre (DLR), 82234 Oberpfaffenhofen, Germany
e-mail: adrian.doicu@dlr.de

Y. Eremin
Lomonosov Moscow State University, Lenin's Hills Moscow, Russia
e-mail: eremin@cs.msu.su

T. Wriedt and Y. Eremin (eds.), *The Generalized Multipole Technique for Light Scattering*, Springer Series on Atomic, Optical, and Plasma Physics 99,
https://doi.org/10.1007/978-3-319-74890-0_3

relating the expansion coefficients of the scattered and incident field is computed. A number of modifications to the conventional null-field method have been proposed, especially to improve the numerical stability in computations for large particles with extreme geometries. These techniques include methods (I) dealing with the numerical stability of the inversion process [6, 9–12], (II) based on accurate computations of the **T**-matrix elements [13–20], (III) relying on formal modifications of the single spherical coordinate-based null-field method [21–24], and (IV) using discrete sources [1, 25]. The fundamentals of the null-field method with discrete sources have been presented in [1], while convergent results for prolate axisymmetric particles with a size parameter of about 100, and oblate axisymmetric particles with a size parameter of about 30 have been reported in [25].

In the first step of our analysis we focus on the discrete sources method and the null-field method with distributed and multiple spherical vector wave functions, and discuss the numerical and theoretical improvements, which are required to handle large and highly aspherical axisymmetric particles. In a second step we present an analytical method for computing the **T**-matrix elements, which may presumably improve the numerical stability of the null-field method with localized spherical vector wave functions.

3.2 Discrete Sources

We consider the scattering by a homogeneous and isotropic particle embedded in a homogeneous, isotropic and nonabsorbing medium. Let D_i be the domain occupied by the particle, D_s the exterior of D_i, S the boundary of D_i (the particle surface), and $\mathbf{n}$ the unit normal vector to S directed into D_s. The wave number in the free space is k_0, while the wave number in domain D_t, $\mathrm{t} = \mathrm{s}, \mathrm{i}$, is $k_\mathrm{t} = k_0\sqrt{\varepsilon_\mathrm{t}\mu_\mathrm{t}}$. Here, ε_t and μ_t are the relative permittivity and permeability of the domain D_t, respectively. The particle is illuminated by an incident field $\mathbf{E}_0$ and $\mathbf{H}_0$, representing an entire solution to the Maxwell equations. The transmission boundary-value problem to be solved consists in the computation of the vector fields $\mathbf{E}_\mathrm{s}$, $\mathbf{H}_\mathrm{s}$ and $\mathbf{E}_\mathrm{i}$, $\mathbf{H}_\mathrm{i}$ satisfying the Maxwell equations

$$\nabla \times \mathbf{E}_\mathrm{t} = \mathrm{j}k_0\mu_\mathrm{t}\mathbf{H}_\mathrm{t}, \quad \nabla \times \mathbf{H}_\mathrm{t} = -\mathrm{j}k_0\varepsilon_\mathrm{t}\mathbf{E}_\mathrm{t}, \tag{3.1}$$

in D_t, $\mathrm{t} = \mathrm{s}, \mathrm{i}$, the two transmission conditions

$$\begin{aligned} \mathbf{n} \times \mathbf{E}_\mathrm{i} - \mathbf{n} \times \mathbf{E}_\mathrm{s} &= \mathbf{n} \times \mathbf{E}_0, \\ \mathbf{n} \times \mathbf{H}_\mathrm{i} - \mathbf{n} \times \mathbf{H}_\mathrm{s} &= \mathbf{n} \times \mathbf{H}_0, \end{aligned} \tag{3.2}$$

$$\frac{\mathbf{r}}{r} \times \sqrt{\mu_\mathrm{s}}\mathbf{H}_\mathrm{s} + \sqrt{\varepsilon_\mathrm{s}}\mathbf{E}_\mathrm{s} = o\left(\frac{1}{r}\right), \text{ as } r \to \infty, \tag{3.3}$$

uniformly for all directions $\mathbf{r}/r$.

As discrete sources, denoted by $\boldsymbol{\Phi}_\alpha^q(k\mathbf{r})$ and $\boldsymbol{\Psi}_\alpha^q(k\mathbf{r})$, with $q = 1, 3$, we consider different types of spherical vector wave functions (SVWF). In particular, $\boldsymbol{\Phi}_\alpha^q$ and $\boldsymbol{\Psi}_\alpha^q$, having the properties:

1. $\nabla \times \boldsymbol{\Phi}_\alpha^q = k\boldsymbol{\Psi}_\alpha^q$ and $\nabla \times \boldsymbol{\Psi}_\alpha^q = k\boldsymbol{\Phi}_\alpha^q$,
2. $\boldsymbol{\Phi}_\alpha^1$ and $\boldsymbol{\Psi}_\alpha^1$ are finite at the origin,
3. $\boldsymbol{\Phi}_\alpha^3$ and $\boldsymbol{\Psi}_\alpha^3$ satisfy the radiation condition,

stand for

1. the localized SVWF (localized multipoles) $\boldsymbol{\Phi}_\alpha^q(k\mathbf{r}) = \mathbf{M}_{mn}^q(k\mathbf{r})$ and $\boldsymbol{\Psi}_\alpha^q(k\mathbf{r}) = \mathbf{N}_{mn}^q(k\mathbf{r})$, where $\alpha = (m, n)$ for $m \in \mathbb{Z}$ and $n \geq \max(1, |m|)$,
2. the distributed SVWF (lowest-order multipoles) $\boldsymbol{\Phi}_\alpha^q(k\mathbf{r}) = \mathbf{M}_{m,|m|+l}^q(k(\mathbf{r} - z_n\mathbf{e}_z))$ and $\boldsymbol{\Psi}_\alpha^q(k\mathbf{r}) = \mathbf{N}_{m,|m|+l}^q(k(\mathbf{r} - z_n\mathbf{e}_z))$, where $\{z_n \mid n \geq 1\}$ is a dense set of points situated on the z-axis, $\mathbf{e}_z$ is the unit vector in the direction of the z-axis, $l = 1$ if $m = 0$ and $l = 0$ if $m \neq 0$, and $\alpha = (m, n)$ for $m \in \mathbb{Z}$ and $n \geq 1$,
3. the multiple SVWF (multiple multipoles) $\boldsymbol{\Phi}_\alpha^q(k\mathbf{r}) = \mathbf{M}_{mn}^q(k(\mathbf{r} - z_p\mathbf{e}_z))$ and $\boldsymbol{\Psi}_\alpha^q(k\mathbf{r}) = \mathbf{N}_{mn}^q(k(\mathbf{r} - z_p\mathbf{e}_z))$, where $\{z_p \mid p = 1, 2, \ldots, N_\mathrm{p}\}$ is a finite set of points (poles) situated on the z-axis, N_p is the number of poles, and $\alpha = (m, n)$ for $m \in \mathbb{Z}$ and $n \geq \max(1, |m|)$.

The explicit expressions of the spherical vector wave functions with an orgin at $\widehat{z}$ along the z-axis read as [25]

$$\begin{aligned} \mathbf{M}_{mn}^{1,3}(k(\mathbf{r} - \widehat{z}\mathbf{e}_z)) = c_n z_n^{1,3}(kR) \big[&\mathrm{j}m\pi_n^{|m|}(\widehat{\theta})(\sin(\theta - \widehat{\theta})\mathbf{e}_r \\ &+ \cos(\theta - \widehat{\theta})\mathbf{e}_\theta) - \tau_n^{|m|}(\widehat{\theta})\mathbf{e}_\varphi \big] \mathrm{e}^{\mathrm{j}m\varphi} \end{aligned} \tag{3.4}$$

and

$$\begin{aligned} \mathbf{N}_{mn}^{1,3}(k(\mathbf{r} - \widehat{z}\mathbf{e}_z)) = c_n \Big\{ &n(n+1)\frac{z_n^{1,3}(kR)}{kR} P_n^{|m|}(\cos\widehat{\theta}) \\ &\times (\cos(\theta - \widehat{\theta})\mathbf{e}_r - \sin(\theta - \widehat{\theta})\mathbf{e}_\theta) + \frac{(kRz_n^{1,3}(kR))'}{kR} \\ &\times \big[\tau_n^{|m|}(\widehat{\theta})(\sin(\theta - \widehat{\theta})\mathbf{e}_r + \cos(\theta - \widehat{\theta})\mathbf{e}_\theta) \\ &+ \mathrm{j}m\pi_n^{|m|}(\widehat{\theta})\mathbf{e}_\varphi\big]\Big\} \mathrm{e}^{\mathrm{j}m\varphi}, \end{aligned} \tag{3.5}$$

where $c_n = 1/\sqrt{2n(n+1)}$, z_n^1 and z_n^3 are the spherical Bessel functions j_n and the spherical Hankel functions of the first kind h_n, respectively, $P_n^{|m|}(\cos\theta)$ the normalized associated Legendre functions, $\tau_n^{|m|}(\theta) = \mathrm{d}P_n^{|m|}(\cos\theta)/\mathrm{d}\theta$, $\pi_n^{|m|}(\theta) = P_n^{|m|}(\cos\theta)/\sin\theta$, $(\mathbf{e}_r, \mathbf{e}_\theta, \mathbf{e}_\varphi)$ the unit vectors in spherical coordinates, (r, θ, φ) and

$$R^2 = \rho^2 + (z - \widehat{z})^2, \quad \sin\widehat{\theta} = \frac{\rho}{R}, \quad \cos\widehat{\theta} = \frac{z - \widehat{z}}{R}.$$

The localized SVWF correspond to $\widehat{z} = 0$ in (3.4) and (3.5), in which case, $R = r$ and $\widehat{\theta} = \theta$.

3.2.1 *Discrete Sources Method for the Transmission Boundary-Value Problem*

The discrete sources method uses the completeness of the systems of tangential vector functions

$$\left\{ \begin{pmatrix} \mathbf{n} \times \boldsymbol{\Phi}_\alpha^{q_t}(k_t\mathbf{r}) \\ -\mathrm{j}\sqrt{\frac{\varepsilon_t}{\mu_t}}\mathbf{n} \times \boldsymbol{\Psi}_\alpha^{q_t}(k_t\mathbf{r}) \end{pmatrix}, \begin{pmatrix} \mathbf{n} \times \boldsymbol{\Psi}_\alpha^{q_t}(k_t\mathbf{r}) \\ -\mathrm{j}\sqrt{\frac{\varepsilon_t}{\mu_t}}\mathbf{n} \times \boldsymbol{\Phi}_\alpha^{q_t}(k_t\mathbf{r}) \end{pmatrix} \right\}$$

on the surface S, i.e., for any tangential field $(\mathbf{e}_0, \mathbf{h}_0)$ and any $\delta > 0$, there exists $N_0 = N_0(\delta)$, such that for all $N > N_0$,

$$\left\| \mathbf{e}_0 + \mathbf{e}_s^N - \mathbf{e}_i^N \right\|_{2S} + \left\| \mathbf{h}_0 + \mathbf{h}_s^N - \mathbf{h}_i^N \right\|_{2S} \leq \delta, \tag{3.6}$$

where $\mathbf{e}_0 = \mathbf{n} \times \mathbf{E}_0$, $\mathbf{h}_0 = \mathbf{n} \times \mathbf{H}_0$, and

$$\begin{aligned} \begin{pmatrix} \mathbf{e}_t^N(\mathbf{r}) \\ \mathbf{h}_t^N(\mathbf{r}) \end{pmatrix} = \sum_{\alpha=1}^{N} a_{t\alpha} \begin{pmatrix} \mathbf{n} \times \boldsymbol{\Phi}_\alpha^{q_t}(k_t\mathbf{r}) \\ -\mathrm{j}\sqrt{\frac{\varepsilon_t}{\mu_t}}\mathbf{n} \times \boldsymbol{\Psi}_\alpha^{q_t}(k_t\mathbf{r}) \end{pmatrix} \\ + b_{t\alpha} \begin{pmatrix} \mathbf{n} \times \boldsymbol{\Psi}_\alpha^{q_t}(k_t\mathbf{r}) \\ -\mathrm{j}\sqrt{\frac{\varepsilon_t}{\mu_t}}\mathbf{n} \times \boldsymbol{\Phi}_\alpha^{q_t}(k_t\mathbf{r}) \end{pmatrix}, \end{aligned} \tag{3.7}$$

with $\mathbf{e}_t = \mathbf{n} \times \mathbf{E}_t$, $\mathbf{h}_t = \mathbf{n} \times \mathbf{H}_t$, t = s, i, $q_s = 3$ and $q_i = 1$. In view of (3.6), the amplitudes of the discrete sources, encapsulated in the $4N$-dimensional vector $\mathbf{x} = [a_{i\alpha}, b_{i\alpha}, a_{s\alpha}, b_{s\alpha}]^T$, can be computed by solving the minimization problem

$$\mathbf{x} = \arg\min \left(\left\| \mathbf{e}_0 + \mathbf{e}_s^N - \mathbf{e}_i^N \right\|_{2S}^2 + \left\| \mathbf{h}_0 + \mathbf{h}_s^N - \mathbf{h}_i^N \right\|_{2S}^2 \right). \tag{3.8}$$

However, this procedure leads to a normal system of equations which is fundamentally unstable for amplitudes determination. To deal with this problem, the point matching method is used instead. Essentially, for a set of P matching points on the particle surface $\{\mathbf{r}_p\}_{p=1}^P$, with $P > N$, we compute the least squares solution $\mathbf{x} = \mathrm{argmin}_{\mathbf{y}} \|\mathbf{A}\mathbf{y} - \mathbf{b}\|^2$, where $\mathbf{A}$ is a $4P \times 4N$ overdetermined matrix, and $\mathbf{b}$ is a $4P$-dimensional vector specified by the values of the incident field at the matching points.

In the null-field method with discrete sources, the internal surface fields $\mathbf{e}_i$ and $\mathbf{h}_i$ are approximated by (3.7), while the expansion coefficients $a_{i\alpha}$ and $b_{i\alpha}$ are computed from the null-field equations

$$\begin{aligned} \frac{\mathrm{j}k_s^2}{\pi} \int_S \Bigg[(\mathbf{e}_i^N(\mathbf{r}) - \mathbf{e}_0(\mathbf{r})) \cdot \begin{pmatrix} \boldsymbol{\Psi}_{\tilde{\alpha}}^3(k_s\mathbf{r}) \\ \boldsymbol{\Phi}_{\tilde{\alpha}}^3(k_s\mathbf{r}) \end{pmatrix} \\ + \mathrm{j}\sqrt{\frac{\mu_s}{\varepsilon_s}} (\mathbf{h}_i^N(\mathbf{r}) - \mathbf{h}_0(\mathbf{r})) \cdot \begin{pmatrix} \boldsymbol{\Phi}_{\tilde{\alpha}}^3(k_s\mathbf{r}) \\ \boldsymbol{\Psi}_{\tilde{\alpha}}^3(k_s\mathbf{r}) \end{pmatrix} \Bigg] \mathrm{d}S(\mathbf{r}) = 0, \end{aligned} \tag{3.9}$$

for $\bar{\alpha} = (-m, n)$ and $\tilde{\alpha} = 1, 2, \ldots, N$. Making use on the vector spherical wave expansion of the incident field,

$$\mathbf{E}_0(\mathbf{r}) = \sum_{\alpha=1}^{N} a_{0\alpha}\mathbf{M}_\alpha^1(k_s\mathbf{r}) + b_{0\alpha}\mathbf{N}_\alpha^1(k_s\mathbf{r}), \tag{3.10}$$

yields

$$\mathbf{Q}^{31}(k_s, k_i) \begin{bmatrix} a_{i\beta} \\ b_{i\beta} \end{bmatrix} = -\mathbf{Q}_0^{31}(k_s, k_s) \begin{bmatrix} a_{0\beta} \\ b_{0\beta} \end{bmatrix}, \tag{3.11}$$

where the entries of the matrix $\mathbf{Q}^{31}(k_s, k_i)$,

$$\mathbf{Q}^{31}(k_s, k_i) = \begin{bmatrix} (Q^{31})_{\alpha\beta}^{11} & (Q^{31})_{\alpha\beta}^{12} \\ (Q^{31})_{\alpha\beta}^{21} & (Q^{31})_{\alpha\beta}^{22} \end{bmatrix} \tag{3.12}$$

are given by

$$\begin{aligned} (Q^{31})_{\alpha\beta}^{11} &= \frac{\mathrm{j}k_s^2}{\pi} \int_S \left[(\mathbf{n} \times \boldsymbol{\Phi}_\beta^1(k_i\mathbf{r})) \cdot \boldsymbol{\Psi}_{\tilde{\alpha}}^3(k_s\mathbf{r}) \right. \\ &\quad \left. + \mathrm{j}m_r(\mathbf{n} \times \boldsymbol{\Psi}_\beta^1(k_i\mathbf{r})) \cdot \boldsymbol{\Phi}_{\tilde{\alpha}}^3(k_s\mathbf{r}) \right] \mathrm{d}S(\mathbf{r}), \\ (Q^{31})_{\alpha\beta}^{12} &= \frac{\mathrm{j}k_s^2}{\pi} \int_S \left[(\mathbf{n} \times \boldsymbol{\Psi}_\beta^1(k_i\mathbf{r})) \cdot \boldsymbol{\Psi}_{\tilde{\alpha}}^3(k_s\mathbf{r}) \right. \\ &\quad \left. + \mathrm{j}m_r(\mathbf{n} \times \boldsymbol{\Phi}_\beta^1(k_i\mathbf{r})) \cdot \boldsymbol{\Phi}_{\tilde{\alpha}}^3(k_s\mathbf{r}) \right] \mathrm{d}S(\mathbf{r}), \end{aligned} \tag{3.13}$$

$$+\mathrm{j}m_r(\mathbf{n}\times\boldsymbol{\Psi}^1_\beta(k_\mathrm{i}\mathbf{r}))\cdot\boldsymbol{\Psi}^3_\alpha(k_\mathrm{s}\mathbf{r})\big]\,\mathrm{d}S(\mathbf{r}),$$

$$(Q^{31})^{22}_{\alpha\beta}=\frac{\mathrm{j}k_\mathrm{s}^2}{\pi}\int_S\big[(\mathbf{n}\times\boldsymbol{\Psi}^1_\beta(k_\mathrm{i}\mathbf{r}))\cdot\boldsymbol{\Phi}^3_\alpha(k_\mathrm{s}\mathbf{r})$$

$$+\mathrm{j}m_r(\mathbf{n}\times\boldsymbol{\Phi}^1_\beta(k_\mathrm{i}\mathbf{r}))\cdot\boldsymbol{\Psi}^3_\alpha(k_\mathrm{s}\mathbf{r})\big]\,\mathrm{d}S(\mathbf{r}), \tag{3.14}$$

with $m_r=\sqrt{\varepsilon_\mathrm{i}/\varepsilon_\mathrm{s}}$ being the relative refractive index of the particle. The matrix $\mathbf{Q}_0^{31}$ has the same structure as the matrix $\mathbf{Q}^{31}$, but it contains as columns the vectors $\mathbf{M}^1_\beta(k_\mathrm{s}\mathbf{r})$ and $\mathbf{N}^1_\beta(k_\mathrm{s}\mathbf{r})$ in place of the vectors $\boldsymbol{\Phi}^1_\beta(k_\mathrm{i}\mathbf{r})$ and $\boldsymbol{\Psi}^1_\beta(k_\mathrm{i}\mathbf{r})$, respectively. The expansion coefficients of the scattered field

$$\mathbf{E}_\mathrm{s}(\mathbf{r})=\sum_{\alpha=1}^{N}a_{\mathrm{s}\alpha}\mathbf{M}^3_\alpha(k_\mathrm{s}\mathbf{r})+b_{\mathrm{s}\alpha}\mathbf{N}^3_\alpha(k_\mathrm{s}\mathbf{r}), \tag{3.15}$$

are computed from Huygens principle in conjunction with the surface fields approximation (3.7). The result is

$$\begin{bmatrix}a_{\mathrm{s}\alpha}\\ b_{\mathrm{s}\alpha}\end{bmatrix}=\mathbf{Q}^{11}(k_\mathrm{s},k_\mathrm{i})\begin{bmatrix}a_{\mathrm{i}\beta}\\ b_{\mathrm{i}\beta}\end{bmatrix}, \tag{3.16}$$

where the matrix $\mathbf{Q}^{11}$ has the same structure as the matrix $\mathbf{Q}^{31}$, but it contains as rows the vectors $\mathbf{M}^1_\alpha(k_\mathrm{s}\mathbf{r})$ and $\mathbf{N}^1_\alpha(k_\mathrm{s}\mathbf{r})$ in place of the vectors $\boldsymbol{\Phi}^3_\alpha(k_\mathrm{s}\mathbf{r})$ and $\boldsymbol{\Psi}^3_\alpha(k_\mathrm{s}\mathbf{r})$, respectively. Combining (3.11) and (3.16) we find that the transition matrix $\mathbf{T}$, relating the scattered field coefficients to the incident field coefficients, is given by

$$\mathbf{T}=-\mathbf{Q}^{11}(k_\mathrm{s},k_\mathrm{i})(\mathbf{Q}^{31}(k_\mathrm{s},k_\mathrm{i}))^{-1}\mathbf{Q}_0^{31}(k_\mathrm{s},k_\mathrm{s}). \tag{3.17}$$

For localized SVWF, $\mathbf{Q}_0^{31}$ is the identity matrix, and (3.17) gives the standard form representation of the transition matrix.

3.2.3 *Algorithm Details*

For axisymmetric particles, the scattering problem is solved independently for each azimuthal modes m. The system of SVWF $\{\boldsymbol{\Phi}^q_{mn}(k\mathbf{r}),\boldsymbol{\Psi}^q_{mn}(k\mathbf{r})\}$ is truncated at an appropriate expansion order N_rank with the following meaning:

1. for the localized SVWF

$$\{\mathbf{M}^q_{mn}(k\mathbf{r}),\ \mathbf{N}^q_{mn}(k\mathbf{r})\mid n=\max(1,|m|),\dots,N_\mathrm{rank}\},$$

N_rank is the order of the localized pole,

of an oblate spheroid, and the image $\widehat{\Sigma}$ of Σ in the complex plane. The dotted circles represent the areas of influence of the poles O_1, O_2, and O_3 situated on the imaginary axis

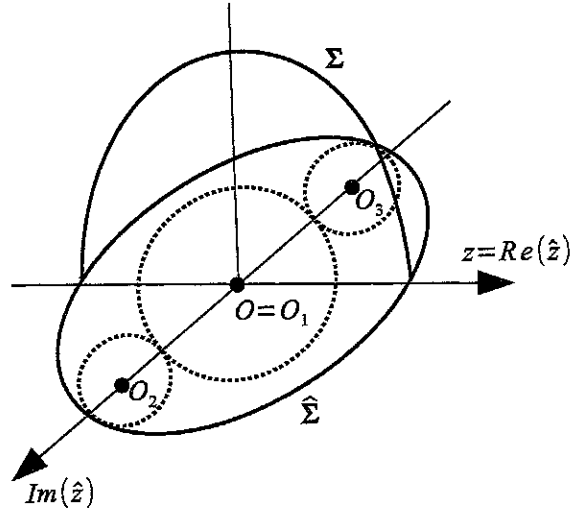

2. for the distributed SVWF

$$\{\mathbf{M}^q_{m,|m|+l}(k(\mathbf{r}-z_n\mathbf{e}_\mathrm{z})),\ \mathbf{N}^q_{m,|m|+l}(k(\mathbf{r}-z_n\mathbf{e}_\mathrm{z}))$$
$$\mid n=1,\dots,N_\mathrm{rank}\},$$

N_rank is number of lowest-order multipoles (discrete sources),

3. for the multiple SVWF

$$\{\mathbf{M}^q_{mn}(k(\mathbf{r}-z_p\mathbf{e}_\mathrm{z})),\ \mathbf{N}^q_{mn}(k(\mathbf{r}-z_p\mathbf{e}_\mathrm{z}))\mid p=1,\dots,N_\mathrm{p},$$
$$n=\max(1,|m|),\dots,N_{\mathrm{rank}p}\},$$

$N_\mathrm{rank}=\sum_p N_{\mathrm{rank}p}$, where $N_{\mathrm{rank}p}$ is the order of the pole p.

The poles are distributed in the complex plane ($\mathrm{Re}\hat{z}$, $\mathrm{Im}\hat{z}$), which is the dual of the azimuthal plane $\varphi=\mathrm{const}$, i.e., (ρ,z) with $\rho\geq 0$ and $z\in\mathbb{R}$ (Fig. 3.1). In the discrete sources method, only lowest-order multipoles are used. For oblate particles, the poles for internal field representation are distributed on the imaginary axis in the interior and exterior of $\widehat{\Sigma}$ (the image of the generatrix Σ in the complex plane), while the poles for scattered field representation are distributed on both the real and imaginary axis in the interior of $\widehat{\Sigma}$. In the null-field method, all types of spherical vector wave functions are considered, and the same poles are used for representing the radiating and the regular system of vector functions in (3.14). For oblate particles, the pole with the largest order is placed at the origin and is called the dominant pole, while the rest of the poles are distributed on the imaginary axis in the interior of $\widehat{\Sigma}$. In both methods, a uniform distribution of the poles along the real axis is used for prolate particles.

identity matrix as regularization matrix, and (III) an a priori regularization parameter choice method based on the size parameter and particle eccentricity. In the null-field method, the matrix inversion is performed by the Gauss elimination method with back-substitution [10], or alternatively, by the block matrix inversion method [11]. To increase the accuracy and efficiency of the Gauss elimination method, the routine has been modified to work in multiple-precision arithmetic with the Multiprecision System (MPFUN90) package [26], and parallelized with OpenMP API.

3.2.4 *Convergence Analysis*

In the null-field method we choose the incident direction along the axis of symmetry of the particle and perform a convergence test over the expansion order $N_{\mathtt{rank}}$. Essentially, we solve the scattering problem for a reference and a lower-order system of SVWF, and check the convergence of the differential scattering cross-sections at a number of scattering angles [7]. The lower-order system of SVWF is chosen as follows: (I) for localized SVWF, the lower-order system is the reference system in which the order of the localized pole is reduced from $N_{\mathtt{rank}}$ to $N_{\mathtt{rank}} - 1$, (II) for distributed SVWF, the lower-order system is the reference system in which the pole placed at the origin is omitted, and finally, (III) for multiple SVWF, the lower-order system is the reference system in which the order of the dominant pole is reduced from $N_{\mathtt{rank1}}$ to $N_{\mathtt{rank1}} - 1$. In the discrete sources method we estimate the residual field at the particle surface for a given configuration of poles. This test which does not require the solution of two scattering problems can be regarded an "internal convergence criterion".

In our analysis we consider spheroids and cylinders, and in order to reduce the numerical instability, we perform the computations using extended- instead of double-precision floating-point variables. For spheroids, we denote by a and b the polar radius and the equatorial radius, respectively, while for cylinders a and b stand for the half-length and the cylinder radius, respectively.

In the first test case we consider a prolate spheroid and a prolate cylinder with a size parameter of $k_{\mathtt{s}}a = 80$ and an aspect ratio of $a/b = 8$. The normalized differential scattering cross-sections are illustrated in Fig. 3.2. In the null-field method with multiple SVWF, the parameters of calculation are $N_{\mathtt{p}} = 31$, $N_{\mathtt{rank}} = 101$, $N_{\mathtt{rank1}} = 11$ and $N_{\mathtt{rank}p} = 3$ for $p \neq 1$ in the case of the spheroid, and $N_{\mathtt{p}} = 31$, $N_{\mathtt{rank}} = 131$, $N_{\mathtt{rank1}} = 11$ and $N_{\mathtt{rank}p} = 4$ for $p \neq 1$ in the case of the cylinder, while in the null-field method with distributed SVWF, the parameters of calculation are $N_{\mathtt{rank}} = 101$ for the spheroid, and $N_{\mathtt{rank}} = 131$ for the cylinder. As it can be seen from Fig. 3.2, the agreement between the discrete sources method and the null-field method with discrete sources is excellent.

In a second test case we consider an oblate spheroid and an oblate cylinder with a size parameter of $k_{\mathtt{s}}b = 50$ and an aspect ratio of $a/b = 1/5$. Because the

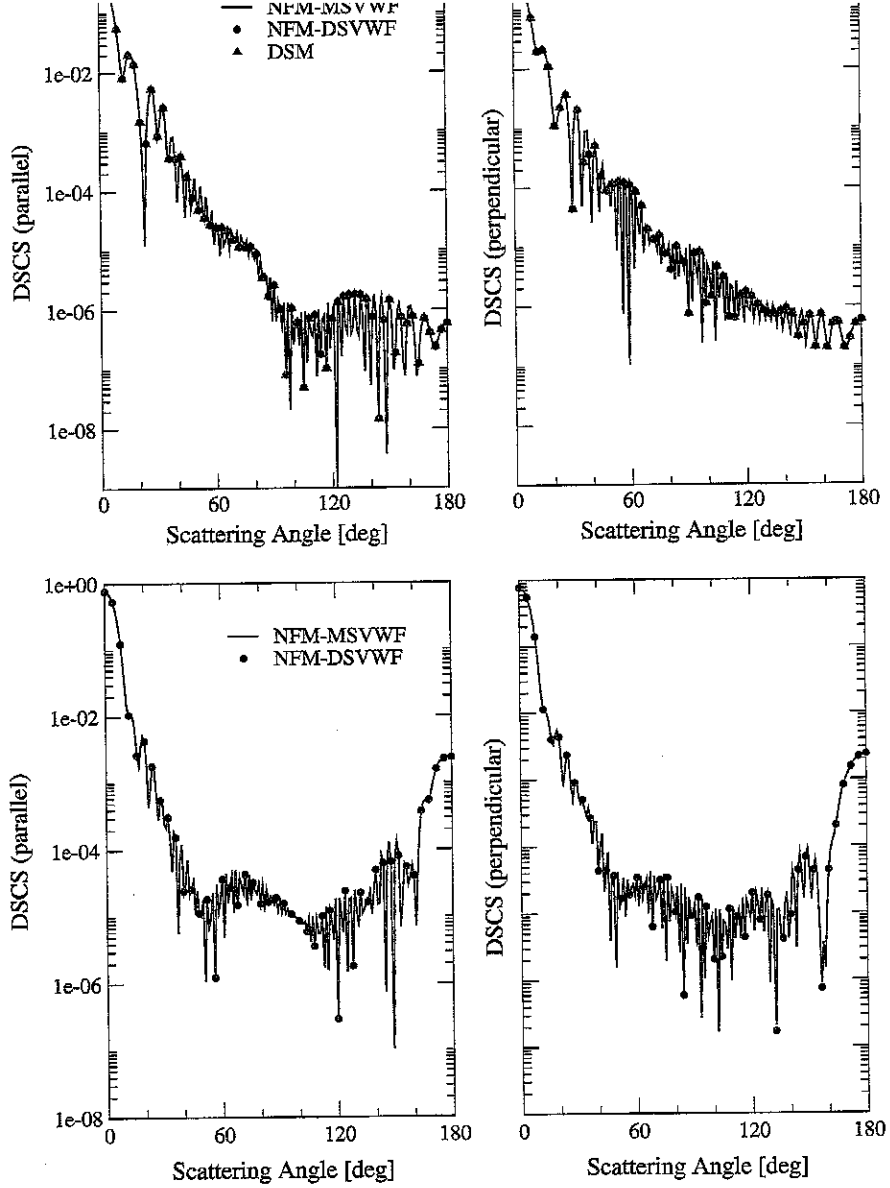

Fig. 3.2 Normalized differential scattering cross-sections computed with the discrete sources method (DSM), and the null-field method with multiple (MSVWF), and distributed (DSVWF) spherical vector wave functions. The results correspond to a prolate spheroid (top panels) and a prolate cylinder (bottom panels) with $m_{\mathtt{r}} = 1.5 + 0.02\mathrm{j}$, $k_{\mathtt{s}}a = 80$ and $k_{\mathtt{s}}b = 10$

discrete sources method, the null-field method with multiple SVWF, and a multiple-precision version of the null-field method with localized SVWF. In the latter case, the calculation of the **Q**-matrix elements and the inversion are performed with multiple-precision arithmetic. The normalized differential scattering cross-sections are illustrated in Fig. 3.3. In the null-field method with multiple SVWF, the parameters of calculation are $N_{\mathrm{p}} = 3$, $N_{\mathrm{rank}} = 96$, $N_{\mathrm{rank1}} = 60$, $N_{\mathrm{rank2,3}} = 18$, $k_{\mathrm{s}}\mathrm{Im}z_1 = 0.0$, and $k_{\mathrm{s}}\mathrm{Im}z_{2,3} = \pm 42$ for the spheroid, and $N_{\mathrm{p}} = 3$, $N_{\mathrm{rank}} = 130$, $N_{\mathrm{rank1}} = 90$, $N_{\mathrm{rank2,3}} = 20$, $k_{\mathrm{s}}\mathrm{Im}z_1 = 0.0$, and $k_{\mathrm{s}}\mathrm{Im}z_{2,3} = \pm 45$ for the cylinder. From Fig. 3.3 we may conclude that the agreement between the different methods is quite good. Coming to the computational efficiency, we mention that for the oblate cylinder, (I) the computational time of the discrete sources method is 7:51 (min:s), (II) the computational times of the null-field method with multiple SVWF are 3:42 (min:s) for the Gauss elimination routine working in extended precision, 3:16 (min:s) for the block matrix inversion routine working in extended precision, and 5:24 (min:s) for the Gauss elimination routine working in multiple precision, and finally, (III) the computational time of the multiple-precision version of the null-field method with localized SVWF is 58:33 (min:sec). Thus, the use of the multiple-precision Gauss elimination routine increases the computational time by a factor of 2, while the multiple-precision version of the null-field method with localized SVWF is extremely inefficient.

In the final test case we consider an oblate spheroid with a size parameter of $k_{\mathrm{s}}b = 80$ and an aspect ratio of $a/b = 1/8$, as well as an oblate cylinder with a size parameter of $k_{\mathrm{s}}b = 70$ and an aspect ratio of $a/b = 1/7$. The results in Fig. 3.4 correspond to the null-field method with multiple SVWF working with a multiple-precision version of the Gauss elimination routine. It should be pointed out that for this test case only this method converges. The parameters of calculation are $N_{\mathrm{p}} = 7$, $N_{\mathrm{rank}} = 264$, $N_{\mathrm{rank1}} = 112$, $N_{\mathrm{rank2,3}} = 40$, $N_{\mathrm{rank4,5}} = 20$, $N_{\mathrm{rank6,7}} = 16$, $k_{\mathrm{s}}\mathrm{Im}z_1 = 0.0$, $k_{\mathrm{s}}\mathrm{Im}z_{2,3} = \pm 55$, $k_{\mathrm{s}}\mathrm{Im}z_{4,5} = \pm 65$, and $k_{\mathrm{s}}\mathrm{Im}z_{6,7} = \pm 75$ for the spheroid, and $N_{\mathrm{p}} = 7$, $N_{\mathrm{rank}} = 268$, $N_{\mathrm{rank1}} = 108$, $N_{\mathrm{rank2,3}} = 40$, $N_{\mathrm{rank4,5}} = 20$, $N_{\mathrm{rank6,7}} = 20$, $k_{\mathrm{s}}\mathrm{Im}z_1 = 0.0$, $k_{\mathrm{s}}\mathrm{Im}z_{2,3} = \pm 45$, $k_{\mathrm{s}}\mathrm{Im}z_{4,5} = \pm 55$, and $k_{\mathrm{s}}\mathrm{Im}z_{6,7} = \pm 65$ for the cylinder. The use of the multiple-precision version of the Gauss elimination routine leads to a relatively high computational times: 86 min for the spheroid and 93 min for the cylinder.

The conclusion of our numerical analysis is that the null-field method with multiple SVWF is superior to the null-field method with distributed SVWF considered in [25]. Another method for improving the numerical stability of the conventional null-field method relies on an analytic computation of the **Q**-matrix elements. This method, which is rather technical, is described in the next section.

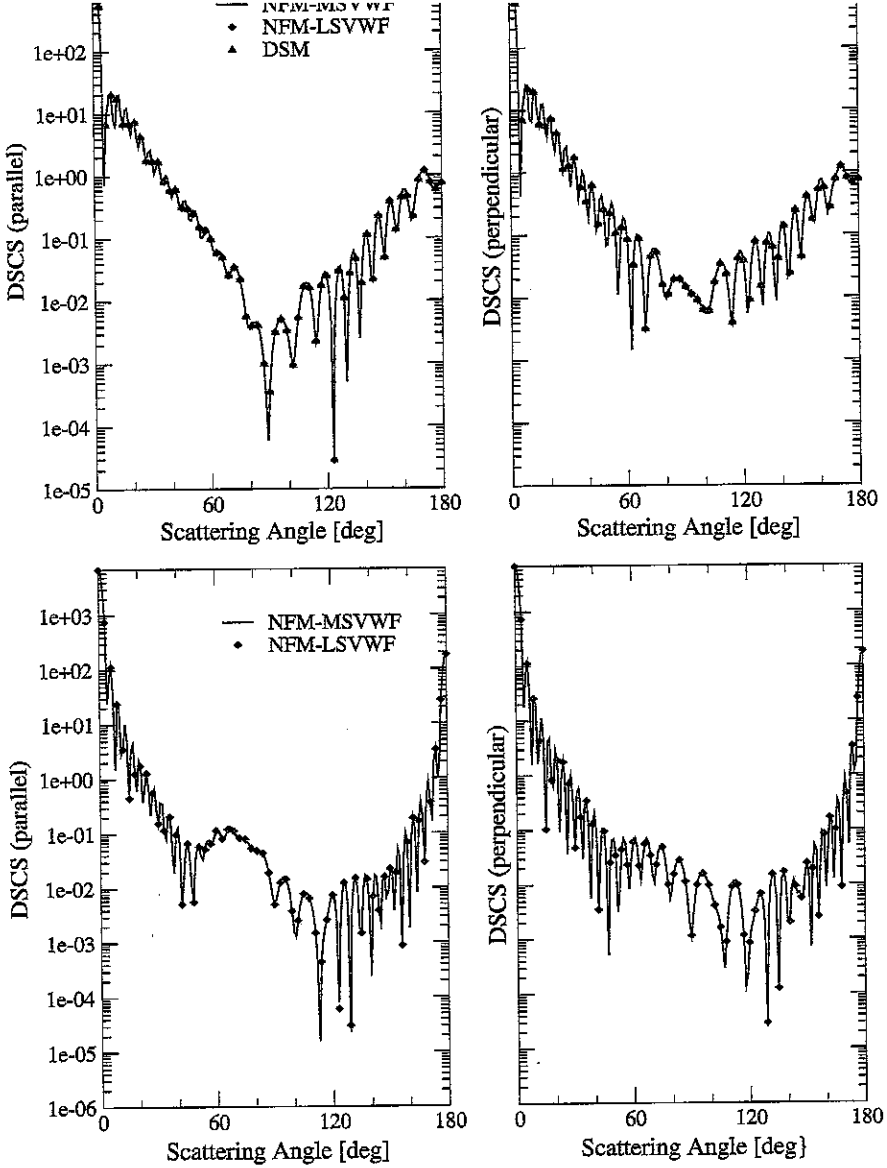

Fig. 3.3 Normalized differential scattering cross-sections computed with the discrete sources method (DSM), and the null-field method with multiple (MSVWF) and localized (LSVWF) spherical vector wave functions. The results correspond to an oblate spheroid (top panels) and an oblate cylinder (bottom panels) with $m_x = 1.5 + 0.02\mathrm{j}$, $k_{\mathrm{s}}a = 10$ and $k_{\mathrm{s}}b = 50$

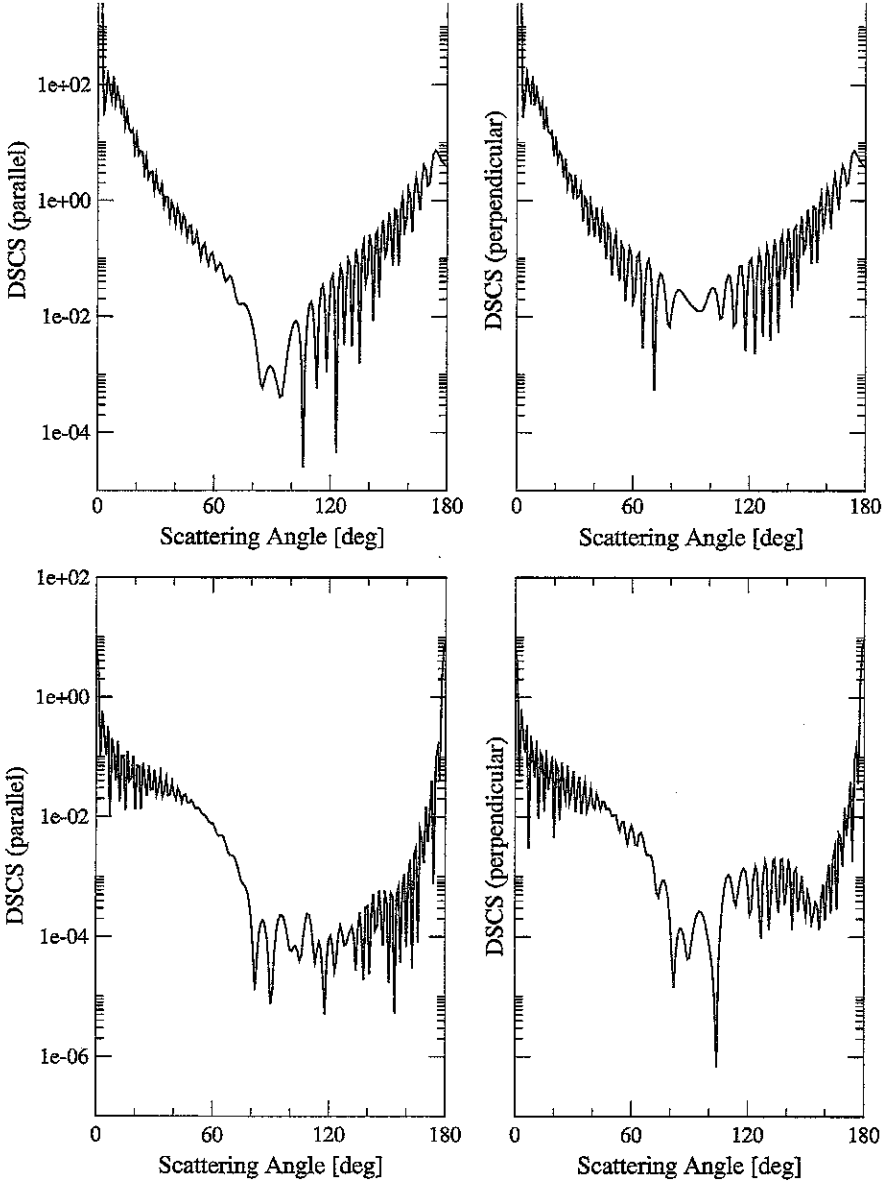

Fig. 3.4 Normalized differential scattering cross-sections computed with the null-field method with multiple spherical vector wave functions. The results correspond to an oblate spheroid with $m_r = 1.5 + 0.02\mathrm{j}$, $k_s a = 10$ and $k_s b = 80$ (top panels) and an oblate cylinder with $m_r = 1.311$, $k_s a = 10$ and $k_s b = 70$ (bottom panels)

Elements

In this section we sketch the main ideas of an analytical method for computing the **Q**-matrix elements in the framework of the null-field method with localized SVWF.

For axisymmetric particles, Somerville et al. [27] have shown that the **Q**-matrix elements can be expressed in terms of six types of integrals. The integrands depend on the regular Riccati-Bessel functions $\psi_n = \psi_n(m_r x) = m_r x j_n(m_r x)$ and their derivatives ψ_n', the Riccati-Hankel functions of the first kind $\xi_n = \xi_n(x) = x h_n(x)$ and their derivatives ξ_n', the unnormalized associated Legendre functions $P_n^{|m|} = P_n^{|m|}(\cos\theta)$, satisfying

$$\int_0^\pi P_n^{|m|}(\cos\theta) P_{n'}^{|m|}(\cos\theta) \sin\theta \, \mathrm{d}\theta = \frac{2}{2n+1} \frac{(n+|m|)!}{(n-|m|)!} \delta_{nn'}, \tag{3.18}$$

and the angular functions $\tau_n^{|m|} = \tau_n^{|m|}(\theta)$. The argument of the Riccati functions is $x = x(\theta) = k_s r(\theta)$, where $r(\theta)$ describes the generatrix in polar coordinates. Assuming that x can be written as $x = x(z(\theta))$, where $z = \cos\theta$, using the decomposition $\xi_n = \psi_n + \mathrm{j}\chi_n$, where $\chi_n(x) = x y_n(x)$ are the irregular Riccati-Bessel functions, and the representations

$$\sin\theta \tau_n^{|m|} = \frac{n\,(n-|m|+1)}{2n+1} P_{n+1}^{|m|} - \frac{(n+1)(n+|m|)}{2n+1} P_{n-1}^{|m|}, \tag{3.19}$$

and

$$X_n' = \frac{n+1}{2n+1} X_{n-1} - \frac{n}{2n+1} X_{n+1}, \tag{3.20}$$

where X_n stands for ψ_n and χ_n, it can be shown that the computation of the six integrals simplifies to the computation of the generic integrals

$$A_{lnkn'k'} = \int_{-1}^{1} \chi_{n'} \psi_{k'} P_n^{|m|} P_k^{|m|} x_z^l \, \mathrm{d}z, \tag{3.21}$$

$$B_{lnkn'k'} = \int_{-1}^{1} \psi_{n'} \psi_{k'} P_n^{|m|} P_k^{|m|} x_z^l \, \mathrm{d}z, \tag{3.22}$$

where $x_z = \mathrm{d}x/\mathrm{d}z$. The indices n' and k' are defined by $n' = n + \overline{n} \geq 0$ and $k' = k + \overline{k} \geq 0$, respectively, and we have (1) $l = 0, 1$, (2) $\overline{n}$, $\overline{k} \in \{-2, -1, 0, 1, 2\}$, $\overline{n} + \overline{k}$ is odd, and (3) $n, k = \max(1, |m|), \ldots, N_{\mathrm{rank}} + 2$.

k, the integrand oscillates around zero and its magnitude varies significantly across the range of integration. Consequently, severe cancellations can occur during the summation step of a Gauss–Legendre quadrature method. To overcome this problem

1. we may perform the computation with increased precision, or we may use the algorithm for summation of floating point numbers as in K-fold working precision developed by Ogita et al. [28],
2. we may remove analytically the terms causing the source of cancellation [14], or finally,
3. we may compute analytically the integral $A_{lnkn'k'}$.

In the following we will be concerned with an analytical computation of the integral $A_{lnkn'k'}$ by using the Gaunt formula for the integral of triple products of associated Legendre functions as suggested in [13]. Other techniques for computing the **Q**-matrix elements can be found in [16–19].

Assuming the representation $x = X\overline{x}$, where X is the size parameter, and making use on the power series representations of the Riccati–Bessel functions

$$\psi_n(x) = \sum_{s=0}^{\infty} \frac{1}{s!}\left(-\frac{1}{2}\right)^s \alpha_{sn} x^{2s+n+1} \tag{3.23}$$

and

$$\chi_n(x) = -\sum_{s=0}^{\infty} \frac{1}{s!}\left(-\frac{1}{2}\right)^s \beta_{sn} x^{2s-n}, \tag{3.24}$$

where

$$\alpha_{sn} = \frac{1}{(2n+2s+1)!!} \tag{3.25}$$

and

$$\beta_{sn} = \begin{cases} (-1)^s\,(2n-2s-1)!! & \text{for } s \le n \\ (-1)^n/(2s-2n-1)!! & \text{for } s > n \end{cases}, \tag{3.26}$$

we obtain

$$A_{lnkn'k'} = -m_r^{k'+1} \sum_{q=0}^{\infty} \gamma_{qn'k'}(m_r) \frac{1}{q!}\left(-\frac{1}{2}\right)^q \times X^{2q+k'-n'+l+1} \int_{-1}^{1} P_n^{|m|} P_k^{|m|} \overline{x}^{2q+k'-n'+1} \overline{x}_z^l \, \mathrm{d}z, \tag{3.27}$$

with

$$\gamma_{qnk}(m_r) = \sum_{s=0}^{q} \frac{q!}{s!(q-s)!} \alpha_{q-s,k} \beta_{sn} m_r^{2(q-s)}. \tag{3.28}$$

has been described in [14]. The method uses a recursion scheme and avoids severe cancellations which may occur when the relative refractive index m_r is close to 1. Setting $s = 2q + k' - n' + 1$ in (3.27) yields

$$A_{lnkn'k'} = -m_r^{k'+1} \sum_{s=k'-n'+1;2}^{\infty} \gamma_{qn'k'}(m_r) \frac{1}{q!}\left(-\frac{1}{2}\right)^q X^{s+l} I_{lsnk}, \tag{3.29}$$

with $q = q(s)$ and

$$I_{lsnk} = \int_{-1}^{1} P_n^{|m|} P_k^{|m|} \overline{x}^s \overline{x}_z^l \, \mathrm{d}z. \tag{3.30}$$

In (3.29), the notation $\sum_{s=s_0;2}^{s_1}$ means that the index s increases from s_0 to s_1 in steps of 2. To compute $A_{lnkn'k'}$ we split the infinite series into a finite series involving negative powers of $\overline{x}$, and an infinite series involving positive powers of $\overline{x}$, i.e.,

$$\sum_{s=k'-n'+1;2}^{\infty} = \sum_{s=k'-n'+1;2}^{s_0} + \sum_{s=s_0+2}^{\infty}, \tag{3.31}$$

where $s_0 = -1$ if $k' - n'$ is even, and $s_0 = -2$ if $k' - n'$ is odd.

The integrals I_{lsnk} depend only on the particle shape, and therefore, they need to be computed only once for a class of particles of similar sizes and refractive indices. The connection to the shape matrix approach, which is based on power series representations of the spherical Bessel and Neumann functions, and the multiplication theorem

$$j_n(X\overline{x}) = X^n \sum_{k=0}^{\infty} \frac{(-1)^k (X^2-1)^k}{k!}\left(\frac{\overline{x}}{2}\right)^k j_{n+k}(\overline{x}),$$
$$y_n(X\overline{x}) = \frac{1}{X^{n+1}} \sum_{k=0}^{\infty} \frac{(X^2-1)^k}{k!}\left(\frac{\overline{x}}{2}\right)^k y_{n-k}(\overline{x}), \tag{3.32}$$

is apparent. Although, from a theoretical point of view, the design of the shape matrix approach by using the multiplication theorem is elegant and ingenious, the final computational relations for the **Q**-matrix elements are identical.

The key point in computing I_{lsnk} is the integral of triple products of associated Legendre functions

$$\int_{-1}^{1} P_n^m P_k^m P_p \, \mathrm{d}z = (-1)^m \frac{2}{2p+1} \overline{a}(m,n,k,p), \tag{3.33}$$

where the coefficients $\overline{a}(m,n,k,p)$ are proportional to the Gaunt coefficients

$$= \frac{2p+1}{2}\frac{(p-m-m')!}{(p+m+m')!}\int_{-1} P_n^m P_k^{m'} P_p^{m+m'}\,\mathrm{d}z \tag{3.34}$$

in the particular case $m' = -m$ and $m \geq 0$, i.e.,

$$\overline{a}(m,n,k,p) = \frac{(k+m)!}{(k-m)!}a(m,n,-m,k,p). \tag{3.35}$$

The coefficients $\overline{a}(m,n,k,p)$ are nonzero for $p = |n-k|, |n-k|+2,\ldots, n+k$, and can be computed by using the downward recurrence relation

$$\varsigma_{p+1}\overline{a}(\cdot,p) - \left(4m^2 + \varsigma_{p+2} + \varsigma_{p+3}\right)\overline{a}(\cdot,p+2) + \varsigma_{p+4}\overline{a}(\cdot,p+4) = 0, \tag{3.36}$$

with the starting values

$$\begin{aligned}\overline{a}(\cdot,n+k) &= \frac{(2n-1)!!(2k-1)!!}{(2n+2k-1)!!}\frac{(n+k)!}{(n-m)!(k-m)!},\\ \overline{a}(\cdot,n+k-2) &= \frac{(2n+2k-3)}{(2n-1)(2k-1)(n+k)}\\ &\quad\times\left[nk - m^2(2n+2k-1)\right]\overline{a}(\cdot,n+k),\end{aligned} \tag{3.37}$$

where $\overline{a}(\cdot,p)$ stands for $\overline{a}(m,n,k,p)$ and

$$\varsigma_p = \frac{\left[4p^2-(n+k+1)^2\right]\left[p^2-(n-k)^2\right]}{4p^2-1}. \tag{3.38}$$

The three-term recurrence formula (3.36) is due to Bruning and Lo [29], and it provides accurate numerical results for all low- and high-degree coefficients.

Let us assume that $\overline{x}$ can be expressed as a finite Legendre series, which approximates a real shape function $\overline{x}_r$ with a truncation error ε, i.e., $\overline{x}_r \approx \overline{x} = \sum_{p=0}^{N_{01}} a_{01p}P_p$, where

$$a_{01p} = \frac{2p+1}{2}\int_{-1}^{1}\overline{x}_r(z)P_p(z)\,\mathrm{d}z, \tag{3.39}$$

and

$$\varepsilon = \int_{-1}^{1}(\overline{x}(z)-\overline{x}_r(z))^2\mathrm{d}z \Big/ \int_{-1}^{1}\overline{x}_r(z)^2\mathrm{d}z. \tag{3.40}$$

In other words, we replace the real shape $\overline{x}_r$ by a pseudo-shape $\overline{x}$, which we then use to compute the **Q**-matrix elements. The same technique has been employed by Petrov et al. in [19]. In Table 3.1 we list the number of terms N_{01} in the finite Legendre series for the superellipse

Table 3.1. Number of terms N_{01} in the Legendre series for a superellipse of eccentricity e and exponent n. The results correspond to the truncation errors $\varepsilon = 10^{-6}$

n \ e	0.8	0.9	0.95
2	10	20	42
4	14	24	48
6	16	32	64
∞	96	166	306

$$\overline{x}_r(\theta) = (\cos^n\theta + e^n\sin^n\theta)^{-1/n}$$

and the truncation error $\varepsilon = 10^{-6}$. The case $n = 2$ corresponds to an ellipse, the cases $n = 4$ and $n = 6$ correspond to a rectangle with rounded corners, and the case $n \to \infty$ corresponds to a rectangle. From this table we see that N_{01} increases with increasing the eccentricity e and the exponent n, and that the method is especially efficient for particles with smooth surfaces.

The computation of I_{lsnk} depends on the sign of s, and we distinguish two cases:

A. Case $s < 0$. As any continuous function defined in the interval $[-1, 1]$ can be expanded in a Legendre series, we set, for any negative s in the finite range $k'-n'+1, k'-n'+3,\ldots,s_0$,

$$\overline{x}^s\,\overline{x}_z^l = \sum_{p=0}^{\infty} a_{lsp}P_p, \tag{3.41}$$

where

$$a_{lsp} = \frac{2p+1}{2}\int_{-1}^{1}\overline{x}^s(z)\overline{x}_z^l(z)P_p(z)\,\mathrm{d}z, \tag{3.42}$$

and $\overline{x}_z = \sum_{p=0}^{N_{01}} a_{01p}P'_p$. We then obtain

$$I_{lsnk} = \sum_{p=|n-k|;2}^{n+k}(-1)^{|m|}\frac{2}{2p+1}a_{lsp}\overline{a}(|m|,n,k,p). \tag{3.43}$$

From (3.43) we see that the vanishing property of Gaunt coefficients implies that only the first $n+k$ terms in expansion (3.41) are required for computing I_{lsnk}.

B. Case $s \geq 0$. Setting $f_{01} = \overline{x}$, and making use on the representation of $\overline{x}$, it is apparent that the product $f_{ls} = \overline{x}^s\,\overline{x}_z^l$ can be expressed as a finite Legendre expansion of the form

$$f_{ls} = \sum_{p=0}^{N_{ls}} a_{lsp}P_p, \tag{3.44}$$

yielding

$$\sum_{p=|n-k|;2} \frac{}{2p+1}$$

The process of computing the expansion coefficients of f_{ls} is based on the following results:

1. The derivative of the finite Legendre series

$$x(z) = \sum_{p=0}^{N} a_p P_p(z)$$

is given by $x_z(z) = \sum_{p=0}^{N-1} b_p P_p(z)$, where in view of the recurrence relation $P'_{p+1} - P'_{p-1} = (2p+1)P_p$, the coefficients b_p are computed as $b_{2p-1} = (4p-1)\sum_{k=p}^{K} a_{2k}$, $p = 1, \ldots, K$ for $N = 2K$ and $N = 2K+1$, and as $b_{2p} = (4p+1)\sum_{k=p}^{K-1} a_{2k+1}$, $p = 0, \ldots, K-1$ for $N = 2K$, and $b_{2p} = (4p+1)\sum_{k=p}^{K} a_{2k+1}$, $p = 0, \ldots, K$ for $N = 2K+1$.
2. The product of the finite Legendre series $x = \sum_{n=0}^{N} a_n P_n$ and $y = \sum_{k=0}^{K} b_k P_k$ is given by $xy = \sum_{p=0}^{N+K} c_p P_p$, where in view of (3.33) and the orthogonality relation of the Legendre polynomials, the coefficients c_p are computed as $c_p = \sum_{n=0}^{N} \sum_{k=|p-n|}^{n+p} a_n b_k \bar{a}(0, n, k, p)$.

The computational process is then organized as follows:

1. compute the expansion coefficients of $\overline{x}_z = f_{10} = \mathrm{d}f_{01}/\mathrm{d}z = \sum_{p=0}^{N_{10}} a_{10p} P_p$, with $N_{10} = N_{01} - 1$, by applying the derivative rule to f_{01},
2. compute the expansion coefficients of f_{0s}, $s \geq 2$, by using the product rule and the recurrence $f_{0s} = f_{0,s-1} f_{01}$, and the expansion coefficients of f_{1s}, $s \geq 1$, by using the product rule and the recurrence $f_{1s} = f_{1,s-1} f_{01}$.

Note that in the case $s = 0$ and $l = 0$ (the case $f_{00} = 1$), we have, $N_{00} = 0$ and $a_{000} = 1$. The numbers of terms in the finite series are $N_{0s} = sN_{01}$ and $N_{1s} = (s+1)N_{01} - 1$.

In the proposed method, the set of expansion coefficients defined by (3.39), i.e., $\{a_{01p} | p = 0, \ldots, N_{01}\}$, and the set of expansion coefficients defined by (3.42), i.e.,

$$\{a_{lsp} | l = 0, 1;\ s = -(N_{\mathrm{rank}} + 3), \ldots, -1;\ p = 0, \ldots, 2N_{\mathrm{rank}} + 4\},$$

describe the particle geometry. They can be computed in the preprocessing step with a desired accuracy, or they can be stored in a database and used as input parameters of the algorithm.

In summary, the analytical method for computing the **Q**-matrix elements involves the following steps:

Laurent series representation of the integrands.
2. Approximate the real shape function $\overline{x}_r$ by a finite Legendre series representing a pseudo-shape function $\overline{x}$.
3. For negative s, expand the product $\overline{x}^s\, \overline{x}_z^l$ in an infinite series of Legendre functions, while for non-negative s, linearize $\overline{x}^s\, \overline{x}_z^l$ by using the product and derivative rule for finite Legendre series.
4. Integrate the linearized terms by using the Gaunt formula for the integral of triple products of associated Legendre functions.

Other techniques for computing I_{lsnk} are summarized below:

1. Assuming that a Taylor expansion of the product $\overline{x}^s(z)\overline{x}_z^l(z)$ around $z = 0$ is available, we may compute the integrals of the form $\int_{-1}^{1} P_n^m(z) P_k^m(z) z^s \, \mathrm{d}z$, $s \geq 0$, by applying the recurrence relation

$$zP_n^m(z) = \frac{n-m+1}{2n+1} P_{n+1}^m + \frac{n+m}{2n+1} P_{n-1}^m \tag{3.46}$$

and the orthogonality relation of the associated Legendre functions, or alternatively, by using the representation

$$z^s = \sum_{p=s,s-2,\ldots} \frac{(2p+1)s!}{2^{(s-p)/2}\,((s-p)/2)!(s+p+1)!!} P_p(z) \tag{3.47}$$

and the integral of triple products of associated Legendre functions.
2. If $r(\theta)$ has a simple representation in terms of trigonometric functions, we may use the relation

$$P_n^m(\cos\theta) = \sum_{k=0}^{n-m} (-1)^k \frac{n!(n+m)!}{k!(n-k)!(n-m-k)!(m+k)!} \times \left(\cos\frac{\theta}{2}\right)^{2n-2k-m} \left(\sin\frac{\theta}{2}\right)^{2k+m}, \quad m \geq 0, \tag{3.48}$$

to reduce the computation of I_{lsnk} to the computation of trigonometric integrals. It seems that this technique has been used by Petrov et al. in [16, 17].

The same approach can be used to compute the **Q**-matrix elements of a non-axisymmetric particle. In this case, the Gaunt coefficients of any degree and order can be computed by using, for example, the recursion scheme developed by Xu [30].

In the first part of this chapter we proved through a numerical analysis that the discrete sources method and the null-field method with distributed and multiple SVWF can be applied to electromagnetic scattering by large axisymmetric particles with extreme geometries. By an appropriate distribution of the poles in the complex plane, the condition number of the matrix to be inverted is decreased, and so, the stability of the computational scheme is increased. In particular, the null-field method with multiple SVWF enabled us to compute the scattering characteristics of oblate particles with a size parameter of 80 and an aspect ratio of 1/8. A drawback of the method is its reduced efficiency; the multiple-precision version of the Gauss elimination routine increases the computational time by a factor of 2 as compared to an extended-precision version. In this regard, we plan to analyze the applicability of an inversion algorithm using floating-point format and a multiplicative correction as described in [31].

In the second part of this chapter we sketched the main ideas of an analytical method for computing the **Q**-matrix elements in the framework of the null-field method with localized SVWF. In summary, the **Q**-matrix elements are expressed as integrals of products of Riccati-Bessel functions, the power series representations of these functions are used to obtain a Laurent series representation of the integrands, and finally, the integrals are computed by using the Gaunt formula for the integral of triple products of associated Legendre functions. Although not yet proved, we expect that this method will avoid the dramatic loss of precision when the integrals in the expressions of the **Q**-matrix elements are computed by a Gauss-Legendre quadrature method.

References

1. A. Doicu, Y. Eremin, T. Wriedt, *Acoustic and Electromagnetic Scattering Analysis Using Discrete Sources* (Academic Press, London, 2000)
2. Y. Eremin, A. Sveshnikov, *The Discrete Sources Method in Electromagnetic Diffraction Problems* (Moscow State University Press, Moscow, 1992)
3. Y. Eremin, Sov. Phys. Dokl. **28**, 451 (1983)
4. C. Hafner, *The Generalized Multipole Technique for Computational Electromagnetics* (Artech House, Boston, 1990)
5. P. Waterman, Proc. IEEE **53**, 805 (1965)
6. P. Waterman, Phys. Rev. D **3**, 825 (1971)
7. P. Barber, S. Hill, *Light Scattering by Particles: Computational Methods* (World Scientific, Singapore, 1990)
8. M. Mishchenko, L. Travis, A. Lacis, *Scattering, Absorption and Emission of Light by Small Particles* (Cambridge University Press, Cambridge, 2002)
9. A. Lakhtakia, V. Varadan, V. Varadan, Appl. Opt. **23**, 3502 (1984)
10. A. Moroz, Appl. Opt. **44**, 3604 (2005)
11. D. Petrov, Y. Shkuratov, G. Videen, Opt. Lett. **32**, 1168 (2007)
12. M. Kahnert, T. Rother, Opt. Express **19**, 11138 (2011)
13. W. Somerville, B. Auguié, E. Le Ru. J. Quant. Spectrosc. Radiat. Trans. **113**, 524 (2012)
16. D. Petrov, G. Videen, Y. Shkuratov, M. Kaydash, J. Quant. Spectrosc. Radiat. Trans. **108**, 81 (2007)
17. D. Petrov, Y. Shkuratov, G. Videen, J. Quant. Spectrosc. Radiat. Trans. **109**, 1474 (2008)
18. D. Petrov, Y. Shkuratov, G. Videen, J. Opt. **12** (2010). http://dx.doi.org/10.1088/2040-8978/12/9/095701
19. D. Petrov, Y. Shkuratov, G. Videen, J. Quant. Spectrosc. Radiat. Trans. **112**, 1636 (2011)
20. M. Mishchenko, L. Travis, Opt. Commun. **109**, 16 (1994)
21. M. Iskander, A. Lakhtakia, C. Durney, IEEE Trans. Antennas Propagat. **31**, 317 (1983)
22. A. Lakhtakia, V. Varadan, V. Varadan, J. Opt. Soc. Am. A **76**, 906 (1984)
23. R. Bates, D. Wall, Phil. Trans. R. Soc. Lond. **287**, 45 (1977)
24. R. Hackman, J. Acoust. Soc. Am. **75**, 35 (1984)
25. A. Doicu, T. Wriedt, Y. Eremin, *Light Scattering by Systems of Particles* (Springer, Berlin, 2006)
26. D. Bailey, ACM Trans. Math. Softw. **21**, 379 (1995)
27. W. Somerville, B. Auguié, E. Le Ru. Opt. Lett. **36**, 3482 (2011)
28. T. Ogita, S. Rump, S. Oishi, SIAM J. Sci. Comput. **26**, 1955 (2005)
29. J. Bruning, Y. Lo, IEEE Trans. Antennas Propagat. **19**, 378 (1971)
30. Y. Xu, J. Comput. Appl. Math. **85**, 53 (1971)
31. S. Rump, Jpn. J. Indust. Appl. Math. **26**, 249 (2009)